



**Linnæus University**

School of Computer Science, Physics and Mathematics

Degree Project

# Modulus of continuity and its application in classifying the smoothness of images.

Behnaz Pirzamanbin

1985-03-22

Subject: Mathematic

Level: advanced level, master

Course code: 5MA11E

### **Abstract**

The problems of de-blurring, de-noising, compression and segmentation are fundamental problems in image processing. Each of these problems can be formulated as a problem to find some approximation of an initial image. To find this approximation one needs to specify the approximation space and in what space the error between the image and its approximation should be calculated.

Using the space of Bounded Variation, BV, became very popular in the last decade. However it was later proved that for a rich variety of natural images it is more effective to use spaces of smooth functions that are called Besov spaces instead of BV. In the previous papers two methods for classifying the smoothness of images were suggested. The DeVore's method based on the wavelet transform and Carasso's method based on singular integrals are reviewed.

The classical definition of Besov spaces is based on the modulus of continuity. In this master thesis a new method is suggested for classifying the smoothness of images based on this definition. The developed method was applied to some images to classify the smoothness of them.

## **Acknowledgments**

First and foremost I offer my sincerest gratitude to my supervisor, Irina Asekritova, who has supported me throughout my thesis with her patience and knowledge. I attribute the level of my Master's degree to her encouragement and effort and without her this thesis would not have been completed or written.

I would like to thank my parents for supporting me throughout all my studies at University and my entire life.

Finally, I thank my best friends for reading my thesis and for their comments and suggestions which considerably improved the quality of this thesis.

# Contents

<b>1</b>	<b>Introduction</b>	<b>4</b>
<b>2</b>	<b>Basic Definitions</b>	<b>8</b>
<b>3</b>	<b>Classifying the smoothness of images using wavelets</b>	<b>10</b>
<b>4</b>	<b>Carasso method of classifying the smoothness of images</b>	<b>13</b>
4.1	Introduction . . . . .	13
4.2	Application of Carasso algorithm . . . . .	15
<b>5</b>	<b>Modulus of continuity</b>	<b>19</b>
5.1	Definition and computation of Modulus of continuity . . . . .	19
5.2	Application of the Modulus of continuity method . . . . .	25
<b>6</b>	<b>Conclusion and Further study</b>	<b>48</b>
6.1	Conclusion . . . . .	48
6.2	Further study . . . . .	50
	<b>References</b>	<b>51</b>

# 1 Introduction

In recent years, important problems in image processing and statistics have been identified. These problems include: denoising, deblurring, compression and segmentation. An image  $f$  can be a noisy image, a messy image (for example, a medical image), a compressed image, a reconstructed image, etc. In these cases, often there is not enough data, or the image is corrupted by noise, or there is no need to reconstruct the exact image  $f$ , as in image compression. Each of these problems can be formulated as a problem of determining a smooth image  $g$  its data approximate the data of an initial image  $f$  by minimizing the following functional,

$$\inf_g (\|f - g\|_X + \lambda \|g\|_Y), \quad (1)$$

To solve this problem one needs to know how to measure the error between functions  $f$  and  $g$  and in which space one estimates  $g$ . The parameter  $\lambda$  determines the relative importance of error and smoothness [1].

Using space of bounded variation,  $BV$ , became very popular in the past decade. However Carraso in [9] and Y. Gousseau and J.-M Morel in [5] claim that  $BV$  space does not work well in deblurring. Furthermore, they also found that most natural images do not belong to  $BV$ , and that a rich variety of images belongs to the scale of Besov space,  $B_{\infty,1}^\alpha$  with  $0.2 < \alpha < 0.7$ .

Moreover, R. A. Devore, B. Jaweth, B. J. Lucier, A. Chambolle and N. Lee, investigated some images through wavelet transform and demonstrated that these images, Figure1-4, belong to  $B_{q,p}^\alpha$  where  $p = q = \frac{2}{1+\alpha}$  with  $0.4 < \alpha < 0.75$  [3].



Figure 1: F-16



Figure 2: Lenna

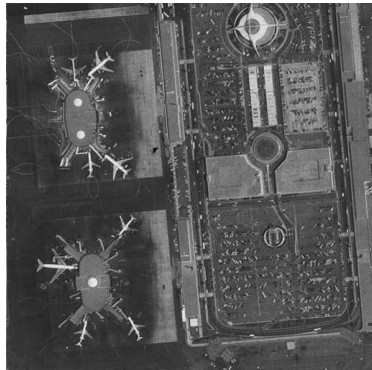


Figure 3: airport



Figure 4: bridge

Y. Meyer noted in [4] that in the problem of denoising, it is very difficult to distinguish between noise and texture. For example, in the mandrill's Beard (Figure 36) plot of function, Figure 5, the reader can see that the function is very oscillated and it is very close to a white noise behavior.

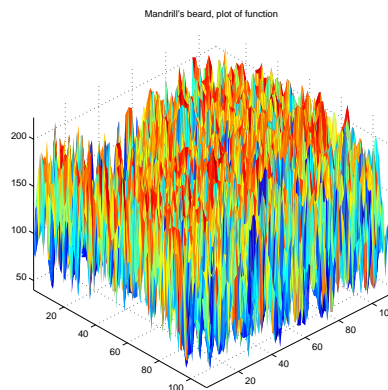


Figure 5: Mandrill's Beard, plot of function

In this case, Y. Meyer suggested to split the images into three parts, "edge", contains the edges and other high priority information, "texture" which contains the low priority information, and "noise",

$$f(x, y) = ed(x, y) + tex(x, y) + n(x, y).$$

One can show that the edge part and the texture part can belong to different spaces.

The reader can see in [4] that only the edge part can lie in the space of bounded variation which is defined by total variation seminorm

$$\int_{R^2} |\nabla f| \, dx dy.$$

However, the texture part as it was shown in [5] is not from  $BV$  due to the fact that it has infinite total variation. These properties lead to the problem of determining the different spaces that contain the image. It is shown later that the Besov space can include most of the textures with the parameter alpha as an indicator of smoothness.

In the first chapter of this thesis, papers of DeVore et al. [2], [1] and [8] are reviewed, in which the authors classified the smoothness of images using wavelets. In the second chapter, Carasso's method of determining the smoothness of images, is explained. The method is applied to find the smoothness of the same images that he considered, "Mandrill" and "Galaxy M51", Figure 6 and 7. The results are analogous to Carasso's result reported in [9].



Figure 6: Galaxy M51

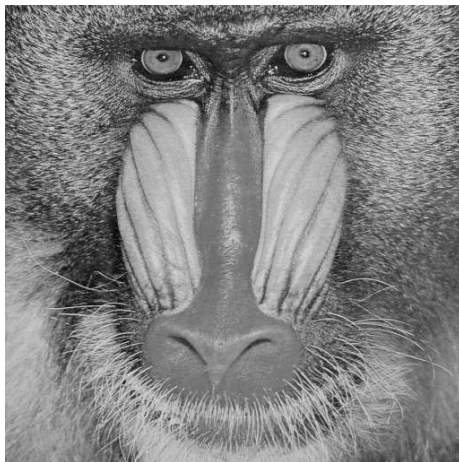


Figure 7: Mandrill

In chapter three, a new method based on Modulus of continuity, is explained. An algorithm is developed and applied to different parts of the images (according to Y. Meyer suggestion) mandrill, Lenna, fruit and boat, Figure 8-11.

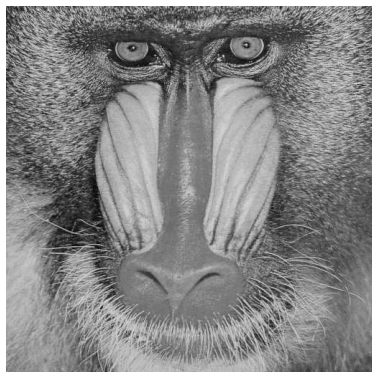


Figure 8: Mandrill



Figure 9: Lenna



Figure 10: Boat

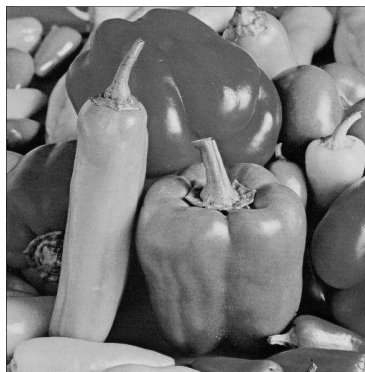


Figure 11: Fruit

At the end, the results are discussed and compared with previous works. In chapters 2, 3 and 4, the author follows the different methods of finding the smoothness of an image to determine the best Besov space for different parts of an image according to reviewed papers and the new method based on modulus of continuity.

## 2 Basic Definitions

Some basic definitions that are used in this master thesis:

**Definition 2.1.** Let  $0 < p \leq \infty$ , and let  $(\Omega, M, \mu)$  be a measure space. The space  $L_p(\Omega)$  is defined as a set of  $f : \Omega \rightarrow \mathbb{R}$  with

$$\|f\|_p = \left( \int_{\Omega} |f|^p d\mu \right)^{1/p} < \infty, \quad 0 < p < \infty \quad (2)$$

and

$$\|f\|_{\infty} := \operatorname{ess\,sup}_{x \in \Omega} |f(x)|, \quad p = \infty.$$

The space  $L_p(\Omega)$  is a linear space, i.e., for each  $\alpha, \beta \in \mathbb{R}$ , if  $f, g \in L_p(\Omega)$  then  $\alpha f + \beta g \in L_p(\Omega)$ .

Note that,

if  $p \geq 1$ , then (2) is a norm with the triangle inequality,  $\|f + g\| < \|f\| + \|g\|$ , and

if  $p < 1$ , then this is not really a norm, it is only a quasi-norm, i.e. in place of the triangle inequality, we have  $\|f + g\|_p \leq 2^{1/p} (\|f\|_p + \|g\|_p)$ .

The definition of Besov space  $B_{q,p}^{\alpha}$  and the definition of modulus of continuity is given,

**Definition 2.2.** Let  $\Omega$  be the unit square in  $\mathbb{R}^2$ . If  $f \in L_p(\Omega)$ ,  $0 < p \leq \infty$ , and  $\omega_r(f, t)_p$ ,  $t > 0$ , denote the modulus of continuity of order  $r$ ,

$$\omega_r(f, t)_p := \sup_{|h| \leq t} \|\Delta_h^r(f, \cdot)\|_{L_p(\Omega(rh))} \quad (3)$$

where  $|h|$  is the Euclidean length of the vector  $h$ ;  $\Delta_h^r$  is the  $r$ th order difference with step  $h \in \mathbb{R}^d$ ; and the norm in (3) is the  $L_p$  norm, on the set  $\Omega(rh) := \{x : x + rh \in \Omega\}$ . Also if  $q = \infty$  and from (3)

$$\omega(t, f)_p \leq Ct^{\alpha}.$$

**Definition 2.3.** (For example, see [1])

If  $\alpha, p, q > 0$ , so  $f$  belongs to Besov space  $B_q^{\alpha}(L_p)$  whenever

$$|f|_{B_{q,p}^{\alpha}} := \left( \int_0^{\infty} (t^{-\alpha} \omega_r(f, t)_p)^q \frac{dt}{t} \right)^{1/q} < \infty, \quad r > \alpha \quad (4)$$

When  $q = \infty$ , the usual change from integral to supremum is made in (4) as following,

$$|f|_{B_{\infty,p}^{\alpha}} := \sup_{t > 0} (t^{-\alpha} \omega_r(f, t)_p)$$

Moreover, norm in  $B_q^{\alpha}(L_p)$  is defined as follows,

$$\|f\|_{B_{q,p}^{\alpha}} := \|f\|_p + |f|_{B_{q,p}^{\alpha}}. \quad (5)$$

In this master thesis  $r = 1$  follows by a restriction for parameter  $\alpha$ ,  $0 < \alpha < 1$ .

Note that when  $t \rightarrow 0$ ,  $\omega(t, f)_p$  also tends to zero. One can measure the smoothness of  $f$  by the rate of  $\omega(t, f)_p \rightarrow 0$ .

$$f \in \mathcal{B}_{\infty, p}^\alpha \Leftrightarrow \omega(f, t)_p = \mathcal{O}(t^\alpha). \quad (6)$$

One can note some properties of Besov space,

- If  $\alpha_1 > \alpha_2$  the function  $f \in \mathcal{B}_{q, p}^{\alpha_1}$  is smoother than function  $f \in \mathcal{B}_{q, p}^{\alpha_2}$ ,
- If  $q_1 > q_2$  the function  $f \in \mathcal{B}_{q_2, p}^\alpha$  is smoother than function  $f \in \mathcal{B}_{q_1, p}^\alpha$ .

More precisely,

$$\mathcal{B}_{q_1, p}^{\alpha_2} \subset \mathcal{B}_{q_2, p}^{\alpha_1},$$

and

$$\mathcal{B}_{q, p}^\alpha \subset \mathcal{B}_{q, s}^\beta$$

Note also, from these embedding it follows

$$\mathcal{B}_{q, p}^\alpha \subset \mathcal{B}_{q, 2}^\beta \subset \mathcal{B}_{\infty, 2}^\beta \subset L_2(\mathbb{R}^2),$$

where  $2/(1 + \alpha) < p \leq 2$  and  $\beta = 1 + \alpha - 2/p$ .

As it will be shown some parts of the picture belong to Besov space with negative smoothness so one needs to consider shifting along smoothness.

In the book [6] of J. Bergh and J. Löfström, the authors define an operator  $J^s$ ,

$$J^s = \mathcal{F}^{-1} \left\{ (1 + |\cdot|^2)^{\alpha/2} \mathcal{F} f \right\} \quad s \in \mathbb{R}$$

The operator  $J^{-s}$  is often called Bessel potential of order  $s$ . The  $\mathcal{F}$  in the Fourier transform of function  $f$ .

It is known that this operator makes "shifting" along the smoothness.

**Theorem 2.1.**  $J^\beta$  is an isomorphism between  $\mathcal{B}_{p, q}^\alpha$  and  $\mathcal{B}_{p, q}^{\alpha-\beta}$ .

### 3 Classifying the smoothness of images using wavelets

In this section, papers [1] and [8] by DeVore et al. concerning data compression using wavelets decomposition are reviewed. The wavelet decomposition is defined as follows,

**Definition 3.1.** A wavelet decomposition of a function  $f$  defined on  $\mathbb{R}^d$  is typically an expression of the form

$$f = \langle f, 2^k \phi \rangle \phi + \sum_{0 \leq k} \sum_{0 \leq j < 2^k} \langle f, 2^k \psi_{j,k} \rangle \psi_{j,k}. \quad (7)$$

where

$$\phi_{j,k}(x) := \phi(2^k(x - j)),$$

and

$$\psi_{j,k}(x) := \psi(2^k(x - j)),$$

are the dyadic dilates (by  $2^k$ ) and translates (by  $j/2^k$ ) of the scaling function  $\phi$  and the wavelet  $\psi$ .

To compress the image one needs to develop an algorithm of constructing a compressed function. DeVore et al. consider approximation  $\tilde{f}_N$  to  $f$  with wavelet expansions

$$\tilde{f}_N = \tilde{c}_{0,0} \phi_{0,0} + \sum_{k \geq 0} \sum_{j \in \mathbb{Z}_k^2} \sum_{\psi \in \Psi} \tilde{c}_{j,k,\psi} \Psi_{j,k}$$

with at most  $N$  nonzero coefficients  $\tilde{c}_{j,k,\psi}$ ; they use  $N$  as the measure of the size of the compressed image  $\tilde{f}_N$ .

To understand how to find coefficients  $\tilde{c}_{j,k,\psi}$ , one needs to find the error metrics to measure the error between  $f$  and  $\tilde{f}$  on some interval  $I \in \mathbb{R}^2$ . The authors use  $L_p(I)$  norm with  $1 \leq p < \infty$  or quasinorm for  $0 < p < 1$ ,

$$\|f - \tilde{f}_N\|_p := \left( \int_I |f - \tilde{f}|^p dx \right)^{1/p}$$

In [1] DeVore et al. claimed that "an image can be compressed well if and only if it is contained in certain smoothness spaces called Besov spaces". To construct the method of compression, one needs to know the smoothness of the image or the Besov space,  $\mathcal{B}_{p,q}^\alpha$  to which the image belongs. Below, DeVore et al's method of classifying the smoothness is described. The error function for the algorithm is introduced as

$$E_N(f)_p := \inf_{\tilde{f}_N} \|f - \tilde{f}_N\|_p,$$

where  $E_N$  is the error of the best approximation of  $f$  by  $\tilde{f}_N$  when the number of coefficients in  $\tilde{f}_N$  does not exceed  $N$ .

It was shown that if  $\frac{1}{q} = \frac{\alpha}{2} + \frac{1}{p}$ ,  $\alpha > 0$ ,  $1 < p < \infty$ , then

$$E_N(f)_p \leq CN^{-\alpha/2}$$

or if  $N = 2^k$

$$\sum_k \left( 2^{\alpha k/2} E_{2^k}(f)_p \right)^q < \infty \Leftrightarrow f \in \mathcal{B}_{q,p}^\alpha$$

Therefore if one knows a wavelet representation of  $f$ , it is possible to calculate  $E_{2^k}(f)_p$  and define a parameter  $\alpha$ , smoothness of  $f$ .

In table 1 the authors reported the smoothness of four considered images, Figure 12-15, using a modified Haar wavelet transform.



Figure 12: F16



Figure 13: Lenna

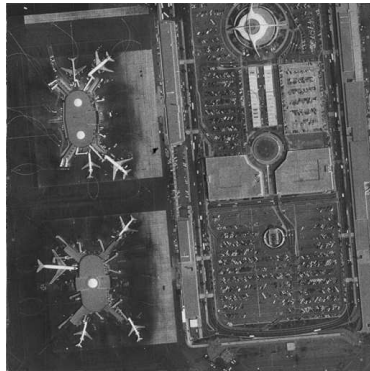


Figure 14: airport



Figure 15: bridge

Table 1: Estimated smoothness of Images

	Lenna	F-16	Bridge	Airport
Estimated $\alpha$	0.599	0.597	0.370	0.306
Estimated $\ f\ _{\mathcal{B}_q^\alpha(L^q(I))}$	0.677	0.676	0.571	0.516
Correlation coefficient	-0.999	-0.993	-0.994	-0.992

## 4 Carasso method of classifying the smoothness of images

### 4.1 Introduction

As it was mentioned in the introduction, Carasso in [9] showed that "most natural images are not of bounded variation" and that a wide class of images belong to the scale of Besov spaces.

In his paper he developed a method to determine a Besov space. To define the smoothness of images, he used the so called Poisson singular integral method which was applied to develop a FFT-based deblurring method. In this chapter, his algorithm is explained. His algorithm was applied to the same images that he used in his paper, M51 galaxy and Mandrill, Figure 16 and 17.

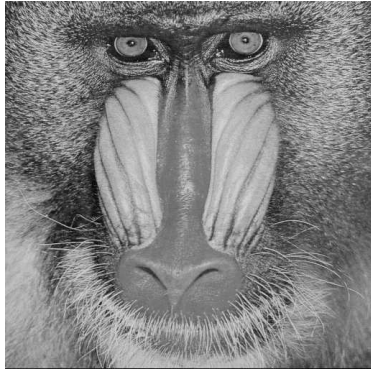


Figure 16: Mandrill



Figure 17: Lenna

As it will be shown later in this chapter, the author obtains the same result as Carasso results in [9].

Some definitions for Carasso method is given below,

**Definition 4.1.** Let  $\psi$  be a Poisson kernel in  $R^2$

$$\psi(x, y, t) = \frac{t}{2\pi(x^2 + y^2 + t^2)^{3/2}}, \quad (x, y) \in R^2.$$

For each  $t > 0$ , define the linear operator  $U^t$ , by

$$U^t f = \int_{R^2} \psi(u, v, t) f(x - u, y - v) dudv. \quad (8)$$

It can be shown that if one defines  $U^0$  to be the identity operator, then for any  $t, s \geq 0$ ,  $U^t U^s = U^{t+s}$ .

Following Carasso, one can state the next theorem

**Theorem 4.1.** Let  $U^t$ ,  $t > 0$ , be the Poisson integral operator (8), and let  $0 < \alpha < 1$ ,  $1 \leq p, q < \infty$ . Then,  $f \in \mathcal{B}_{q,p}^\alpha$  if and only if

$$\int_0^\infty \left( t^{-\alpha} \|U^t f - f\|_p \right)^q dt/t < \infty.$$

For  $q = \infty$ , we have  $f \in \mathcal{B}_{\infty,p}^\alpha$  if and only if

$$\sup_{t>0} t^{-\alpha} \|U^t f - f\|_p < \infty.$$

**Theorem 4.2.** (corollary) Let  $f \in \mathcal{B}_{q,p}^\alpha$ , with  $2/(1 + \alpha) < p \leq 2$ , and let  $\beta = 1 + \alpha - 2/p$ . Then, in the  $L^2$  norm

$$\sup_{t>0} t^{-\beta} \|U^t f - f\|_2 < \infty.$$

For any image  $f(x, y)$  in  $L_1(\mathbb{R}^2)$ , one can use Fourier transform on  $U^t f$ .  $\mathcal{F}(U^t f)$  is considered as convolution between  $\psi$  and  $f$ . By the convolution property,

$$\mathcal{F}(f * g) = \mathcal{F}(f)\mathcal{F}(g),$$

one obtains

$$\mathcal{F}(U^t f) = \hat{\psi}(\gamma, \vartheta, t) \cdot \hat{f}(\gamma, \vartheta),$$

where the Fourier transform of the Poisson Kernel is

$$\hat{\psi}(\gamma, \vartheta, t) = e^{-t|\bar{\xi}|} \text{ as } \bar{\xi} = (\gamma, \vartheta)$$

so that  $\hat{\psi}(\gamma, \vartheta, t) = e^{-t\sqrt{\gamma^2 + \vartheta^2}}$  we denote  $\sqrt{\gamma^2 + \vartheta^2}$  by  $\rho$ . Finally,

$$\mathcal{F}(U^t f) = e^{-t\rho} \hat{f}(\gamma, \vartheta) \text{ , } \rho = \sqrt{\gamma^2 + \vartheta^2}.$$

From the above calculations, one can produce sequence of positive numbers  $(t_n, \mu_n)$ ,  $t_n = 0.5(0.95)^n$  and

$$\mu_n = \frac{\|U^{t_n} f - f\|_1}{\|f\|_1} \text{ as } t_n \rightarrow 0.$$

Moreover from the theorem 4.1,

$$f \in \mathcal{B}_{\infty,p}^\alpha \Leftrightarrow \sup_{t>0} t^{-\alpha} \|U^t f - f\|_p < \infty.$$

Carasso suggested to define smoothness in the following way;

If all these sequences lies below the curve  $\mu(t) = Ct^\alpha$ , as  $0 < t \leq \bar{t}$ ,  $C > 0$  and  $0 < \alpha < 1$ , then

$$\|U^t f - f\|_1 \leq C \|f\|_1 t^\alpha \text{ as } t \rightarrow 0.$$

## 4.2 Application of Carasso algorithm

The considered function  $f$  defined on  $[0, 1] \times [0, 1]$ , by reflecting the image one can make  $f$  periodic.[10] By using the Poisson summation formula, one obtains

$$U^t f = \sum_{\gamma, \vartheta=-\infty}^{\infty} e^{-t\rho} \hat{f}(\gamma, \vartheta) e^{2\pi i(x\gamma + y\vartheta)}, \quad t > 0, \rho = \sqrt{\gamma^2 + \vartheta^2}.$$

Now let

$$f_N = \sum_{\gamma, \vartheta=-N}^N e^{-t\rho} \hat{f}(\gamma, \vartheta) e^{2\pi i(x\gamma + y\vartheta)}, \quad t > 0, \rho = \sqrt{\gamma^2 + \vartheta^2}.$$

Since  $L^p(\Omega) \subset L^1(\Omega)$ ,  $p > 1$  one can apply this for any  $f \in L^p$  and by choosing  $N$  large,  $\|U^t f - f_N\|_p$  can be small. The method uses the FFT algorithms for any image  $f(x, y)$ , to find the Fourier coefficients  $\hat{f}(\gamma, \vartheta)$ . By applying the filter  $(e^{-t\rho} - 1)$  on  $\hat{f}$ , an inverse FFT yields an accurate approximation to  $U^t f - f$ , for each small  $t > 0$ . To determine the Besov space one needs to find the constant  $C$  and  $\alpha$  such that  $\|U^{t_n} f - f\|_p \leq C \|f\|_p t^\alpha, 0 < t \leq \bar{t}$  [9]. The least square fitting method is used to find the best fit. The reader can find the method in following definition.

**Definition 4.2.** Given  $m$  data

$$(x_i, y_i), i = 1, \dots, m$$

one wants to find the coefficients  $\alpha$  and  $\beta$  such that

$$f(x) = \alpha x + \beta$$

is a least square fit to our data.

One chooses  $\alpha$  and  $\beta$  such that they minimize

$$\sum_{i=1}^m r_i^2.$$

where  $r_i$  is the residual for the data  $(x_i, y_i)$ .

The difference between the known data and the fit function,

$$\begin{aligned} r_i &= y_i - f(x_i) \\ &= y_i - (\alpha x_i + \beta) \end{aligned}$$

So one minimizes  $\rho$ ,  $\rho(\alpha, \beta) = \|r\|_2^2$  with respect to  $\alpha$  and  $\beta$

$$\frac{\partial \rho}{\partial \alpha} \Big|_{\beta=\text{constant}} = 0$$

and

$$\frac{\partial \rho}{\partial \beta} \Big|_{\alpha=\text{constant}} = 0.$$

If one writes the equation for the fit in matrix form

$$\begin{bmatrix} x_1 & 1 \\ x_2 & 1 \\ \vdots & \vdots \\ x_m & 1 \end{bmatrix} [\alpha \quad \beta] = \begin{bmatrix} y_1 \\ y_2 \\ \vdots \\ y_m \end{bmatrix} \text{ or } X\theta = Y,$$

where

$$X = \begin{bmatrix} x_1 & 1 \\ x_2 & 1 \\ \vdots & \vdots \\ x_m & 1 \end{bmatrix}, \quad [\alpha \quad \beta] = \theta, \quad Y = \begin{bmatrix} y_1 \\ y_2 \\ \vdots \\ y_m \end{bmatrix}.$$

One can compute  $\rho(\alpha, \beta) = \|r\|_2^2$ , where  $r = Y - X\theta$

$$\begin{aligned} \rho(\alpha, \beta) = \|r\|_2^2 = r^T r &= (Y - X\theta)^T (Y - X\theta) \\ &= Y^T Y - (X\theta)^T Y - Y^T (X\theta) + \theta^T X^T X \theta \\ &= Y^T Y - 2Y^T (X\theta) + \theta^T X^T X \theta. \end{aligned}$$

Minimizing  $\rho$  with respect to  $\theta$

$$\frac{\partial \rho}{\partial \theta} = -2X^T Y + 2X^T X \theta = 0,$$

one obtains the estimated parameters

$$\hat{\theta} = (X^T X)^{-1} X^T Y.$$

The line  $f(x) = \hat{\alpha}x + \hat{\beta}$  is fitted to the data  $y$ . [7]

The Carasso method is applied to mandrill and galaxy M51, as you can see in next pages. The same result for parameters  $\alpha$  and  $C$ , in addition same Besov space are concluded as Carasso reported in [9].

**Example 4.1. Mandrill:**

*First of all, the algorithm is applied to mandrill (see Figure18),*

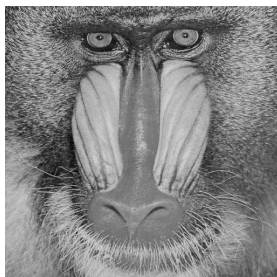


Figure 18: Mandrill

*After using Matlab computation and also applying the least square fitting to the main plot, a plot is obtained which one can see in 19, here the  $\mu(t)$  is the blue curve for  $-6 < \log t < -1$ . The red line is the least square fit to the  $\mu(t)$ . From these calculations  $C = 0.3239$  and  $\alpha = 0.3053$  are obtained which mean that the image belongs to  $\mathcal{B}_{\infty,2}^{0.3053}$ .*

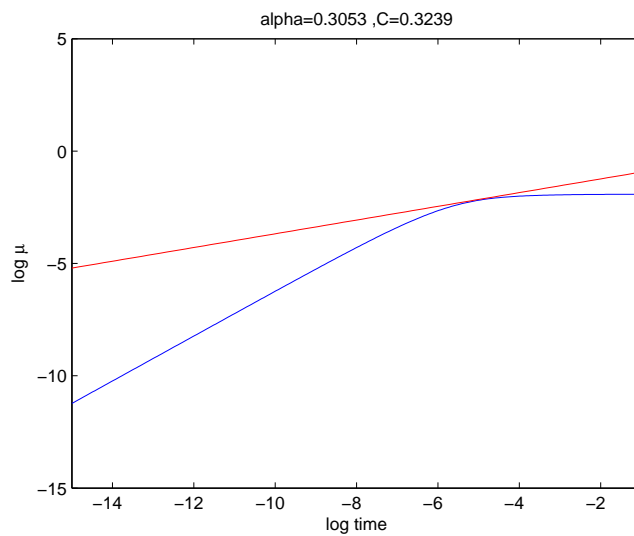


Figure 19: PSI on Mandrill

**Example 4.2. M51:**

Then, another image Figure(20), galaxy M51, was considered,



Figure 20: M51

The reader can see the result below in plot (21),  $C = 0.8176, \alpha = 0.5227$  and  $\mathcal{B}_{\infty,2}^{0.5227}$  is obtained.

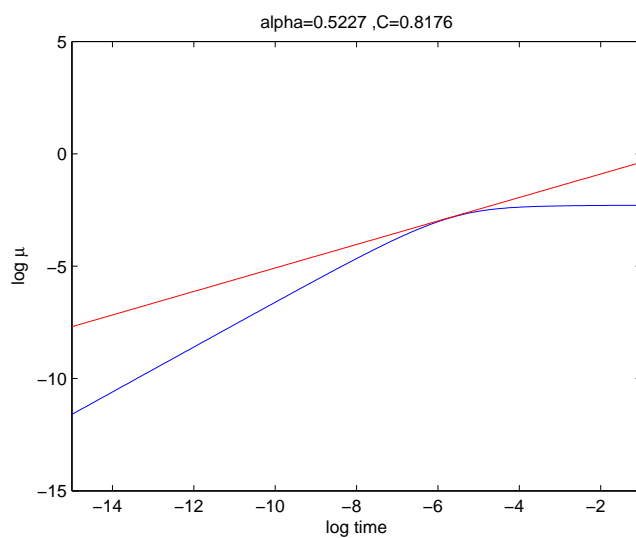


Figure 21: PSI on M51

Similar to plot(19) the red line is the least square fit to  $\mu(t)$  for  $t$  which is closed to zero.

## 5 Modulus of continuity

### 5.1 Definition and computation of Modulus of continuity

Modulus of continuity is another method that is used in this thesis to find the smoothness of an image and specify the image space. First of all, a definition of modulus of continuity in the one dimensional case which is more identifiable and intelligible is considered. Then it is extended into the two dimensional case. For the given images modulus of continuity are calculated by using MATLAB.

From the definition 3 in section 2; it follows that modulus of continuity  $\omega(f, t)$  in the spaces  $L_\infty(\Omega)$  and  $L_1(\Omega)$  are given by the formulas

$$\omega(t, f)_\infty = \sup_{|h| \leq t} \|f(x+h) - f(x)\|_{L_\infty(\Omega_h)},$$

and

$$\omega(t, f)_1 = \sup_{|h| \leq t} \|f(x+h) - f(x)\|_{L_1(\Omega_h)}.$$

where  $\Omega_h = \{x : x+h \in \Omega\}$ . Note in one dimensional case  $\Omega = (0, 1)$  and in two dimensional case is square  $(0, 1) \times (0, 1)$ . The author explain by some examples how to calculate the Modulus of continuity,  $\omega(f, t)$  by using MATLAB.

**Example 5.1.** Let  $f(t) = t^\alpha$ ,  $0 \leq t \leq 1$ ,  $n = 2^{10}$ .

To calculate  $\omega(f, t)$  by using MATLAB we consider vectors

$$\bar{t} = (t_1, \dots, t_n),$$

where  $t_k = t(\frac{k-1}{n})$ , and

$$\bar{f} = (f_1, \dots, f_n),$$

where  $f_k = f(t_k)$ , and  $k = 1, \dots, [\frac{n}{2}]$

$$\omega(f, t)_\infty = \max_{1 \leq l \leq k} \max_{1 \leq k \leq n-l} |f_{k+l} - f_k|$$

and

$$\omega(f, t) = \max_{1 \leq l \leq k} \sum_{k=1}^{n-l} |f_{k+l} - f_k|.$$

In the Figure 22 the reader can see the plot of the considered functions  $f(t) = t^\alpha$  with different  $\alpha = 0.2, 0.5, 0.7$  for number of samples  $n = 2^{10}$ , also second and third plots are the plots of  $\omega(f, t)_1$  and  $\omega(f, t)_\infty$  for  $t \in [0, 1/4]$  in the log-log scale. Moreover the plot of  $\omega(f, t)$  in the space of  $L_\infty$  is very similar to behavior of the function  $f(t)$ .

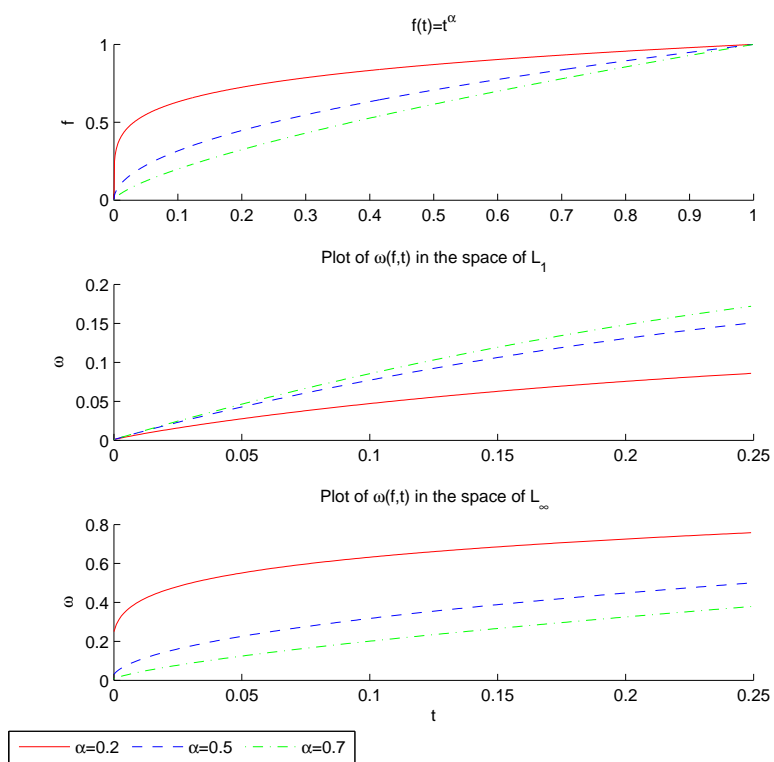


Figure 22: Plots of  $f = t^\alpha$  and the modulus of continuity in the space  $L_1$  and  $L_\infty$  for 256 samples for three different values of  $\alpha$ .

In the second example a step function is considered,

**Example 5.2.** Let  $f$  be the step function,

$$f(t) = \begin{cases} 0.5 & 0 < t < 0.2 \\ 3.5 & 0.2 \leq t < 1 \end{cases}$$

The same method that is described in the first example is used to compute the modulus of continuity of the step function  $f$ . In the Figure 23 one can see the result of MATLAB computation.

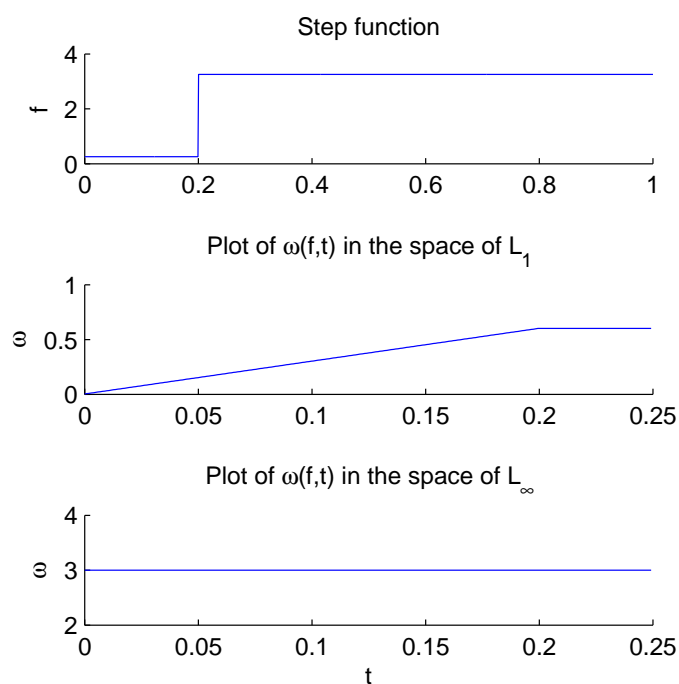


Figure 23: The first plot is  $f$  and in the second plot the reader can see the modulus of continuity in log-log scale in the space  $L_1$  norm. The last plot is  $\log \omega$  vs.  $\log t$ , in the space  $L_\infty$  norm.

In the two dimensional case the algorithm of calculating  $\omega(f, t)$  works in the analogous way.

The function  $f$  that is defined on the square  $[0, 1] \times [0, 1]$  is given by the matrix  $f = (f_{k,l})_{k,l=1}^n$  with  $f_{k,l} = f(\frac{k-1}{n}, \frac{l-1}{n})$ . From the equation 3, one computes the differences

$$|f(x+h, y+h') - f(x, y)|,$$

where  $x = \frac{k-1}{n}$ ,  $y = \frac{l-1}{n}$  and  $h = \frac{r-1}{n}$ ,  $h' = \frac{s-1}{n}$  are such that  $|h|, |h'| \leq t$ . Then we calculate  $\omega(f, t)$  with  $t = t(\frac{m-1}{n})$ ,  $m = 1, \dots, [\frac{n}{2}]$  in  $L_\infty$  and  $L_1$  spaces using formulas,

$$\omega(t, f)_\infty = \max_{\substack{1 \leq s \leq k, \\ 1 \leq r \leq l}} \max_{\substack{1 \leq k \leq n-s, \\ 1 \leq l \leq n-r}} |f_{k+s, l+r} - f_{k, l}|,$$

and

$$\omega(t, f)_1 = \max_{\substack{1 \leq s \leq k, \\ 1 \leq r \leq l}} \sum_{\substack{1 \leq k \leq n-s, \\ 1 \leq l \leq n-r}} |f_{k+s, l+r} - f_{k, l}|.$$

A function  $f \in \mathcal{B}_{\infty, p}^\alpha$  whenever

$$\omega(f, t)_p \leq Ct^\alpha \quad (9)$$

This inequality is equivalent to

$$\log \omega(t, f) \leq \log C + \alpha \log t \quad (10)$$

To specify to what space belong the function, one needs to:

- calculate the modulus of continuity,  $\omega(f, t)$ ,
- plot the graph of  $\omega(f, t)$  in log-log scale,
- use least square method to find the the parameters  $C$  and  $\alpha$  ,i.e, to find the best approximation of  $\log \omega(f, t)$  by the linear function

$$\log C + \alpha \log t$$

for small values of arguments.

The  $\alpha$  is the smoothness and  $C$  is the norm. Therefore from definition 2.3 of Besov space it follows that  $f \in \mathcal{B}_{p, q}^\alpha$  with the norm  $\|f\|_{q, p}^\alpha \leq C$ . The algorithm above can be used only for the function  $f \in \mathcal{B}_{p, q}^\alpha$  with  $\alpha \in (0, 1)$ . However some images are described by the functions that oscillate a lot. Such functions can belong to the Besov space with negative smoothness. To classify the smoothness in this case we need to use theorem 2.1 (see section (2)) to make "shifting" along the smoothness.

According to theorem 2.1, the operator  $J^{-s}$  is an isomorphism between two spaces,  $\mathcal{B}_{p, q}^\alpha$  and  $\mathcal{B}_{p, q}^{\alpha+s}$ . Recall that

$$J^{-s} f = \mathcal{F}^{-1} \left\{ \frac{\mathcal{F}(f)}{(1+k^2)^{\frac{s}{2}}} \right\} \quad (11)$$

To classify the smoothness of a given function  $f \in \mathcal{B}_{\infty, p}^\alpha$  with  $\alpha \in (-1, 0)$  the function  $g$  is considered as below

$$g = J^{-s} f = \mathcal{F}^{-1} \left\{ \frac{\mathcal{F}(f)}{(1+k^2)^{\frac{s}{2}}} \right\}.$$

It is clear that  $g \in \mathcal{B}_{q,p}^{\alpha+s}$ . Therefore one can classify the smoothness of  $g$  by the method is described above, i.e, parameters  $C$  and  $\beta$  are determined such that

$$\omega(g, t) \leq Ct^\beta \quad 0 < \beta < 1.$$

For example if  $s = 1$  and  $g = \mathcal{F}^{-1} \left\{ \frac{\mathcal{F}(f)}{(1+k^2)^{\frac{1}{2}}} \right\}$ ,

$$\omega(g, t) \leq Ct^\beta \Leftrightarrow g \in \mathcal{B}_{\infty,p}^\beta,$$

therefore  $f \in \mathcal{B}_{\infty,p}^{\beta-1}$ .

To use shifting (11) one needs to calculate the Fourier transform. To calculate the Fourier transform of the given function the Fast Fourier Transform (FFT) is used. Below some technical details of using FFT is explained. First, one dimensional case is considered then a function  $f$  is defined on the interval  $[0, 1]$ . For the given function  $f$ , a vector  $\bar{f} = (f_1, f_2, \dots, f_n)$  is considered. Then  $\bar{f}$  can be written as

$$\bar{f} = \sum_{k=1}^n c_k e_k,$$

where  $e_1, e_2, \dots, e_n$  are vectors define by formulas

$$\begin{aligned} e_1 &= \{1, 1, \dots, 1\} \\ e_2 &= \left\{1, e^{i\frac{1}{n}2\pi}, \dots, e^{i\frac{n-1}{n}2\pi}\right\} \\ e_3 &= \left\{1, e^{2i\frac{1}{n}2\pi}, \dots, e^{2i\frac{n-1}{n}2\pi}\right\} \\ &\vdots \\ e_n &= \left\{1, e^{(n-1)i\frac{1}{n}2\pi}, \dots, e^{(n-1)i\frac{n-1}{n}2\pi}\right\} \end{aligned}$$

Using the inner product

$$\langle f, g \rangle = \sum f_k \bar{g}_k,$$

one gets,

$$\begin{aligned} \langle e_k, e_l \rangle &= 1 + e^{ik\frac{2\pi}{n}} e^{-il\frac{2\pi}{n}} + \dots + e^{ik\frac{2\pi}{n}(n-1)} e^{-il\frac{2\pi}{n}(n-1)} \\ &= 1 + e^{(k-l)i\frac{2\pi}{n}} + \dots + e^{(k-l)i\frac{2\pi}{n}(n-1)} \\ &= \frac{1 - e^{i(k-l)2\pi}}{1 - e^{i(k-l)\frac{2\pi}{n}}} \\ &= 0. \end{aligned}$$

And moreover

$$\begin{aligned} \langle e_k, e_k \rangle &= 1 + e^{ik\frac{2\pi}{n}} e^{-ik\frac{2\pi}{n}} + \dots + e^{ik\frac{2\pi}{n}(n-1)} e^{-ik\frac{2\pi}{n}(n-1)} \\ &= n. \end{aligned}$$

and one can write

$$f = \sum_{k=1}^n \frac{\langle f, e_k \rangle}{\langle e_k, e_k \rangle} e_k = \sum_{k=1}^n \frac{\langle f, e_k \rangle}{n} e_k,$$

The program FFT calculate the vector

$$\mathcal{F}(f) = FFT[f] = \left\{ \underbrace{\langle f, e_1 \rangle}_{\hat{f}_1}, \underbrace{\langle f, e_2 \rangle}_{\hat{f}_2}, \dots, \underbrace{\langle f, e_n \rangle}_{\hat{f}_n} \right\} \quad (12)$$

In conclusion,

$$f = \sum_{k=1}^n \frac{(FFT[f])_k}{n} e_k.$$

The method is similar for the two dimensional case. One assumes that an image is described by a function of two variables on the square  $[0, 1] \times [0, 1]$ . A discretization  $\bar{f} = (f_{k,l})_{k,l=1}^n$  of  $f$  is considered, where

$$f_{k,l} = f\left(\frac{k-1}{n}, \frac{l-1}{n}\right).$$

Then  $\bar{f}$  can be written as

$$\bar{f} = \sum_{k,l=1}^n c_{k,l} e_{k,l},$$

where

$$e_{k,l} = \left\{ e^{i(k-1)x_r} e^{i(l-1)y_s} \right\}_{r,s=1}^n$$

with  $x_r = \frac{r-1}{n}2\pi, y_s = \frac{s-1}{n}2\pi$  and

$$c_{k,l} = \frac{\langle f, e_{k,l} \rangle}{\langle e_{k,l}, e_{k,l} \rangle} = \frac{\langle f, e_{k,l} \rangle}{n^2} = \frac{(FFT2[f])_{k,l}}{n^2}. \quad (13)$$

Note assuming that a considered function is periodic it is useful to change formulas(13) by the following,

$$c_{k,l} = \frac{(FFT2[f])_{k,l}}{\min(k-1, n-(k-1))^2 + \min(l-1, n-(l-1))^2}$$

To obtain an accurate result, the algorithm applied for the given image. Finally to classify the smoothness of an image the best result is taken in account the following factors,

1. correlation coefficient: calculate the correlation coefficient of  $\omega(f, t)$  and  $Ct^\alpha$ , choose the one which has a bigger correlation (close to one),
2. error: calculate the error in the  $L_2$  space between the  $\omega$  and  $Ct^\alpha$ , choose the one close to zero,
3. plot: plot the graph of the modulus of continuity  $\omega(f, t)$ , if  $\omega$  grows fast, i.e. reaches its maximum after a few iteration, the function  $f$  oscillate alot to classifying the smoothness one needs to use shifting theory.

From the next page, the Modulus of continuity method is applied on the different images.

## 5.2 Application of the Modulus of continuity method

The Modulus of continuity method is applied as it was explained above to the following pictures, Figure 24-27.

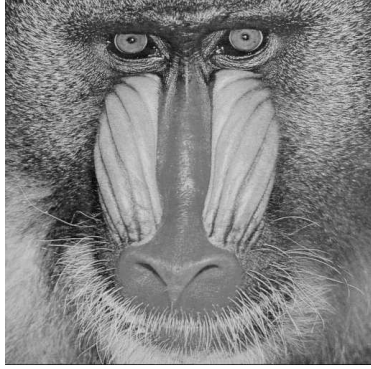


Figure 24: Mandrill



Figure 25: Lenna



Figure 26: Boat

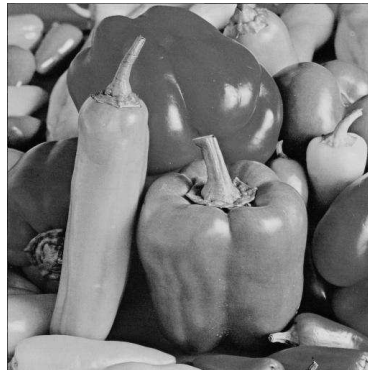


Figure 27: Fruit

The algorithm takes the different parts from each image to compare different texture and their related space. For that reason the algorithm calculates the Modulus of continuity,  $\omega(f, t)$ , of each part of the image and makes 5 different shiftings because of the reason explained before. A line is fitted to  $\omega$  by the least square method. The least square method gives the parameters  $\alpha$  and  $C$  where  $\alpha$  is the smoothness and  $C$  is the norm in each specified space. According to the result of the least square method, one can plot the  $\omega$  vs.  $Ct^\alpha$  and from all three factors, error, correlation coefficient, and plot, the best  $\alpha$  and  $C$  are obtainable.

In the examples below, the results for different parts of the images are provided,

**Example 5.3.** *For the Lenna image, different parts are chosen according to texture and shape,*

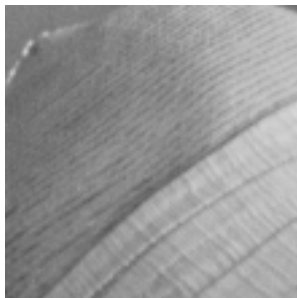


Figure 28: Lenna Hat

Table 2: Estimated smoothness of Lenna Hat part in  $L_2$

smoothness ( $\alpha$ )	-0.2069
norm	1.6238
correlation coefficient	0.9991
error	0.7276

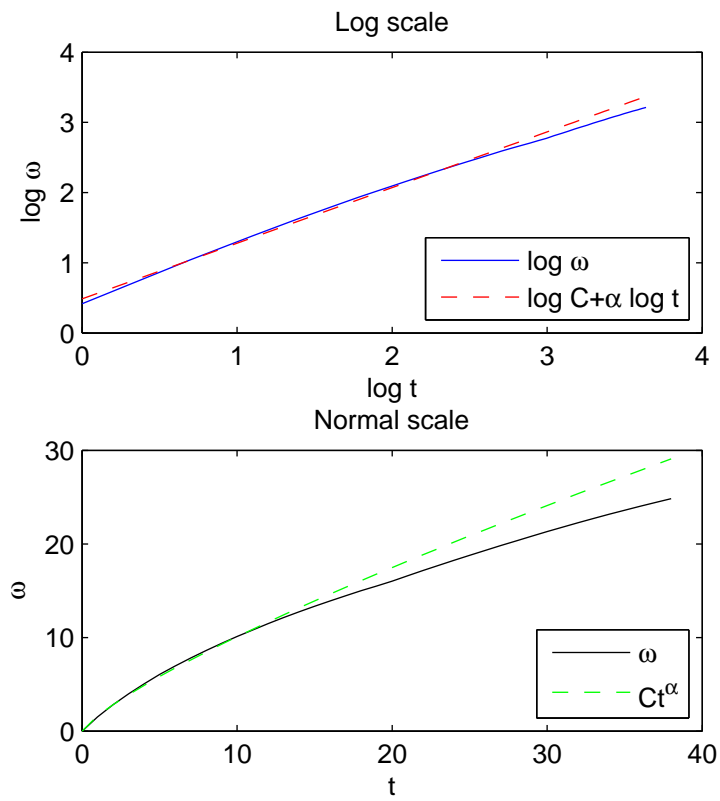


Figure 29: In the first plot, the red dash line is a least square fit to the log scale of  $\omega$ , the green line, with respect to the small  $t$ . In the second plot one can see the fit of  $\omega$ , black line and  $Ct^\alpha$ , dashed green line, where  $\alpha = -0.2069$  and  $C = 1.6238$  with the  $\mathcal{B}_{\infty,2}^{-0.2069}$

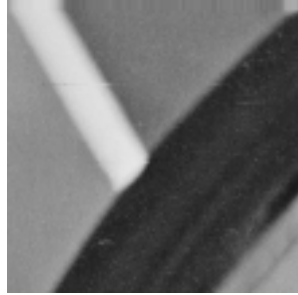


Figure 30: Lenna Geometric

Table 3: Estimated smoothness of Lenna geometric part in  $L_2$

smoothness ( $\alpha$ )	0.2851
norm	5.1774
correlation coefficient	0.9981
error	3.1414

---

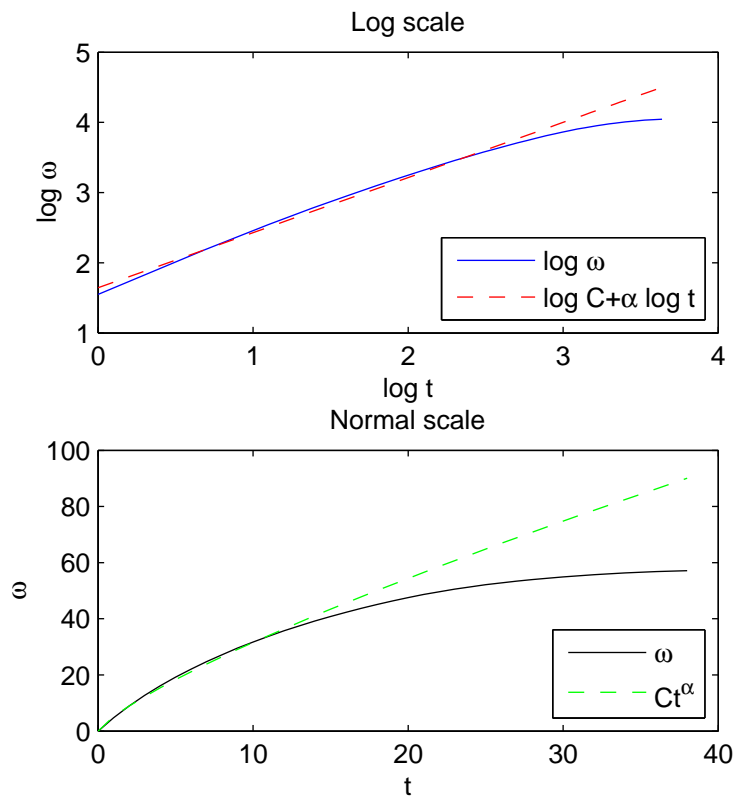


Figure 31: In first plot, red dash line is least square fit to the log scale of  $\omega$ , the green line, with respect to the small  $t$ . In the second plot one can see the fit of  $\omega$ , black line and  $Ct^\alpha$ , dashed green line, where  $\alpha = 0.2851$  and  $C = 5.1774$  with the  $\mathcal{B}_{\infty,2}^{0.2851}$



Figure 32: Lenna Hat's Hair

Table 4: Estimated smoothness of Lenna hat's hair part in  $L_2$

smoothness ( $\alpha$ )	-0.2765
norm	1.7845
correlation coefficient	0.9985
error	0.8285

---

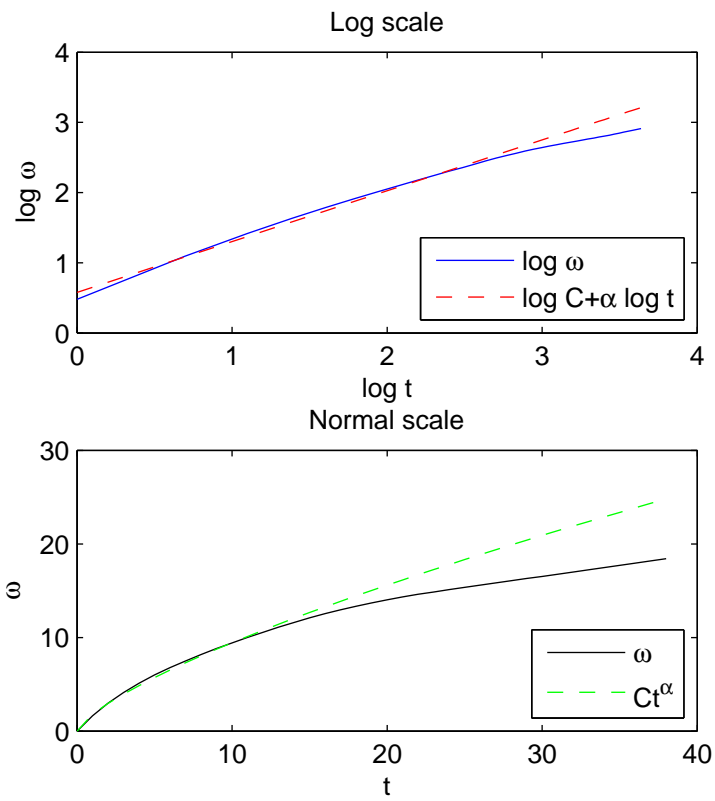


Figure 33: In the first plot, the red dashed line is a least square fit to the log scale of  $\omega$ , the green line, with respect to the small  $t$ . In the second plot one can see the fit of  $\omega$ , black line and  $Ct^\alpha$ , dashed green line, where  $\alpha = -0.2765$  and  $C = 1.7845$  with the  $\mathcal{B}_{\infty,2}^{-0.2765}$

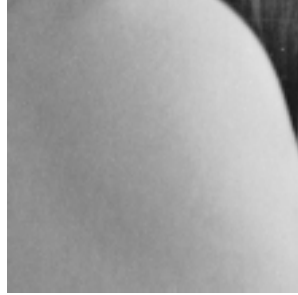


Figure 34: Lenna Skin

Table 5: Estimated smoothness of Lenna skin part in  $L_2$

smoothness ( $\alpha$ )	0.2651
norm	3.2316
correlation coefficient	0.9970
error	2.2372

---

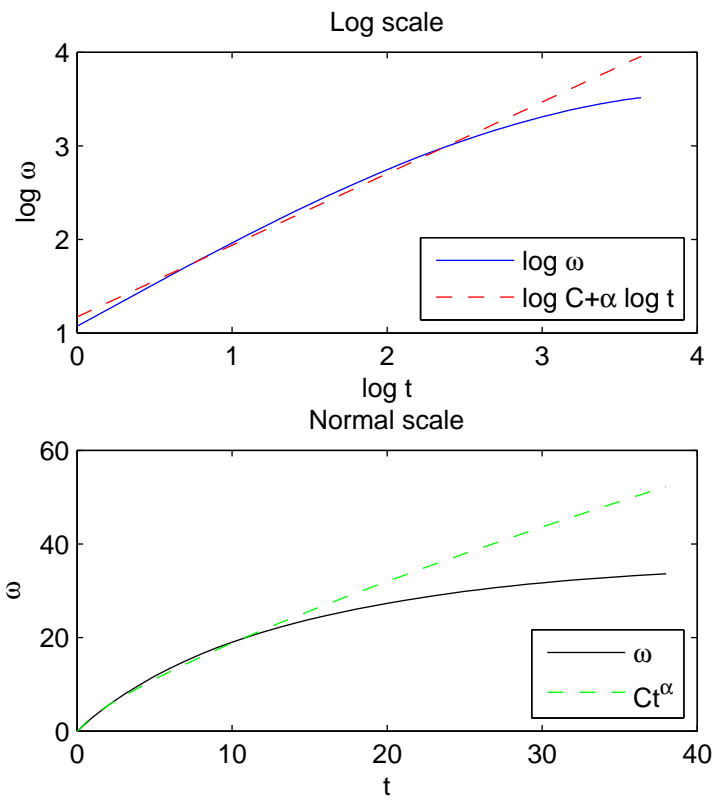


Figure 35: In the first plot, the red dashed line is a least square fit to the log scale of  $\omega$ , the green line, with respect to the small  $t$ . In the second plot one can see the fit of  $\omega$ , black line and  $Ct^\alpha$ , dashed green line, where  $\alpha = 0.2651$  and  $C = 3.2316$  with the  $\mathcal{B}_{\infty,2}^{0.2651}$

**Example 5.4.** *It also chooses different part of mandrill image to compare the space of the textures,*

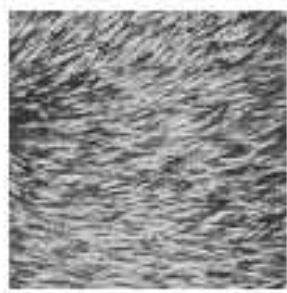


Figure 36: Mandrill Beard

Table 6: Estimated smoothness of Mandrill beard part in  $L_2$

smoothness ( $\alpha$ )	-0.3165
norm	2.1240
correlation coefficient	0.9991
error	0.6269

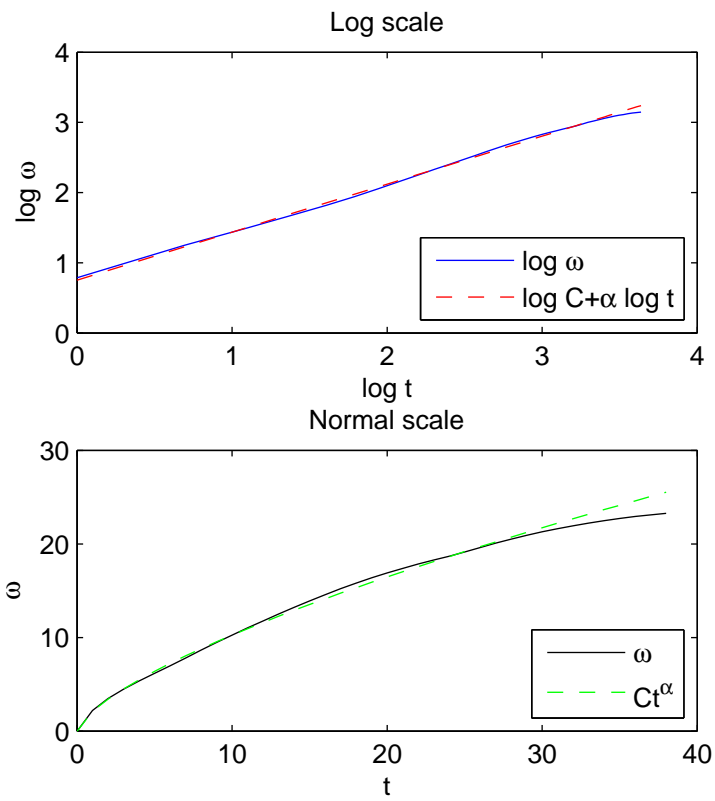


Figure 37: In the first plot, the red dashed line is a least square fit to the log scale of  $\omega$ , the green line, with respect to the small  $t$ . In the second plot one can see the fit of  $\omega$ , black line and  $Ct^\alpha$ , dashed green line, where  $\alpha = -0.3165$  and  $C = 2.1240$  with the  $\mathcal{B}_{\infty,2}^{-0.3165}$



Figure 38: Mandrill Nose

Table 7: Estimated smoothness of Mandrill nose part in  $L_2$

smoothness ( $\alpha$ )	0.2200
norm	3.6159
correlation coefficient	0.9998
error	0.5009

---

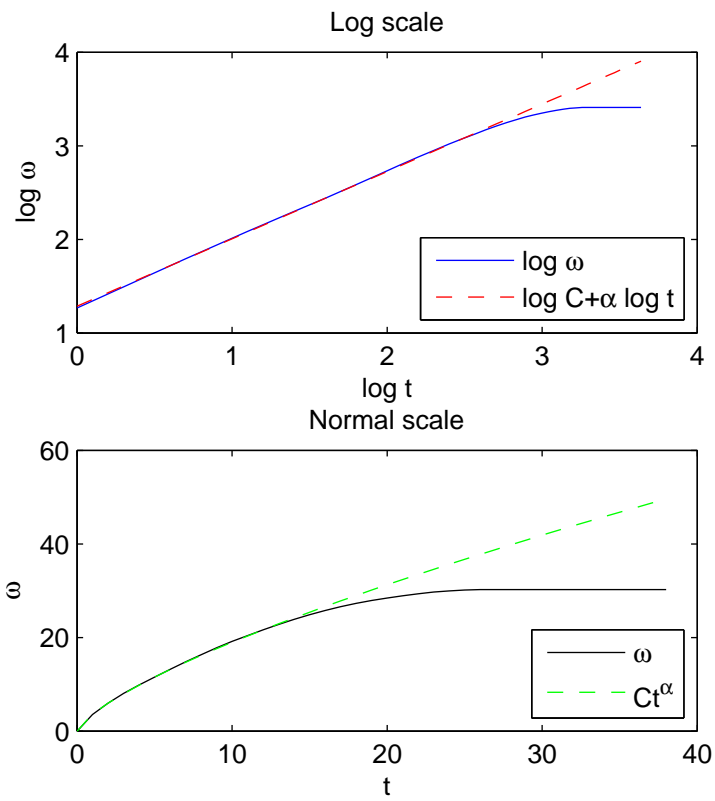


Figure 39: In the first plot, the red dashed line is a least square fit to the log scale of  $\omega$ , the green line, with respect to the small  $t$ . In the second plot one can see the fit of  $\omega$ , black line and  $Ct^\alpha$ , dashed green line, where  $\alpha = 0.2200$  and  $C = 3.6159$  with the  $\mathcal{B}_{\infty,2}^{0.2200}$



Figure 40: Mandrill Hair

Table 8: Estimated smoothness of Mandrill hair part in  $L_2$

smoothness ( $\alpha$ )	-0.3351
norm	1.4625
correlation coefficient	0.9986
error	0.5382

---

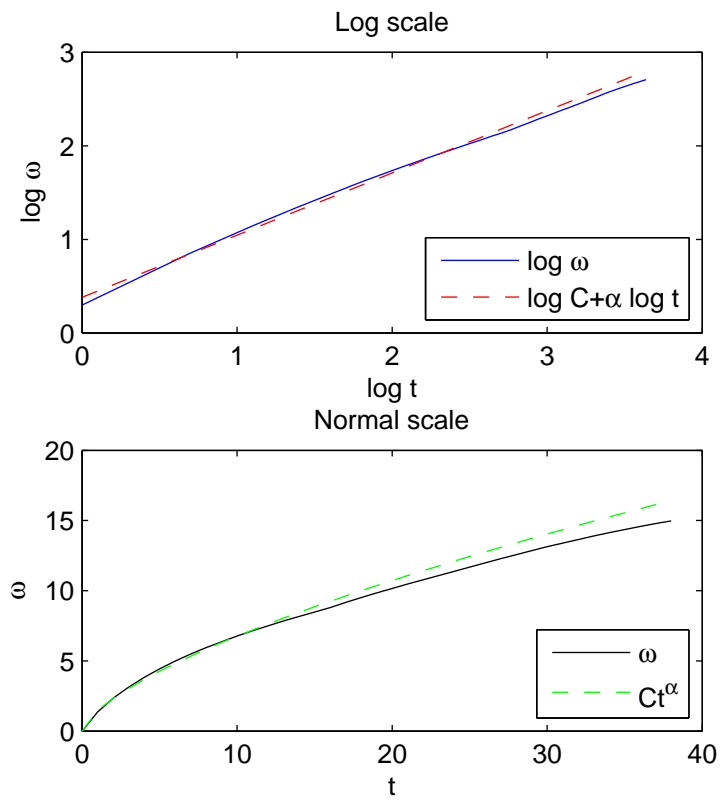


Figure 41: In the first plot, the red dashed line is a least square fit to the log scale of  $\omega$ , the green line, with respect to the small  $t$ . In the second plot one can see the fit of  $\omega$ , black line and  $Ct^\alpha$ , dashed green line, where  $\alpha = -0.3351$  and  $C = 1.4625$  with the  $\mathcal{B}_{\infty,2}^{-0.3351}$

**Example 5.5.** Here it computes the different parts of fruit image,



Figure 42: Fruit Geometric

Table 9: Estimated smoothness of Fruit geometric part in  $L_2$

smoothness ( $\alpha$ )	0.2052
norm	4.4407
correlation coefficient	0.9972
error	2.1810

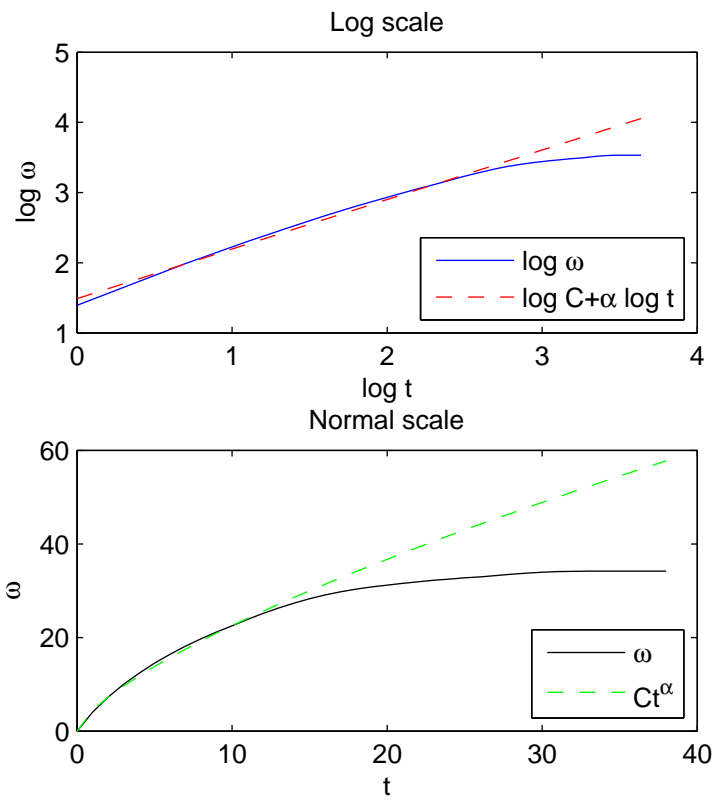


Figure 43: In the first plot, the red dashed line is a least square fit to the log scale of  $\omega$ , the green line, with respect to the small  $t$ . In the second plot one can see the fit of  $\omega$ , black line and  $Ct^\alpha$ , dashed green line, where  $\alpha = 0.2052$  and  $C = 4.4407$  with the  $\mathcal{B}_{\infty,2}^{0.2052}$



Figure 44: Fruit Skin

Table 10: Estimated smoothness of Fruit skin part in  $L_2$

smoothness ( $\alpha$ )	-0.3148
norm	0.5956
correlation coefficient	0.9600
error	0.4465

---

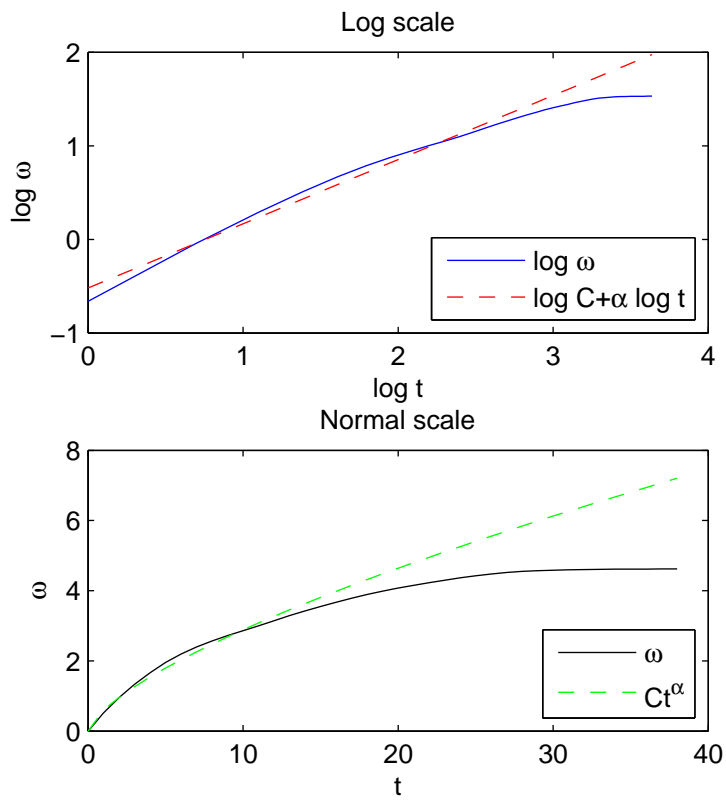


Figure 45: In the first plot, the red dashed line is a least square fit to the log scale of  $\omega$ , the green line, with respect to the small  $t$ . In the second plot one can see the fit of  $\omega$ , black line and  $Ct^\alpha$ , dashed green line, where  $\alpha = -0.3148$  and  $C = 0.5956$  with the  $\mathcal{B}_{\infty,2}^{-0.3148}$

**Example 5.6.** For the last example, the boat image is chosen. It contains the wavy sea and a geometric part of the boats to compare the different parts of this image, with itself and also other results,

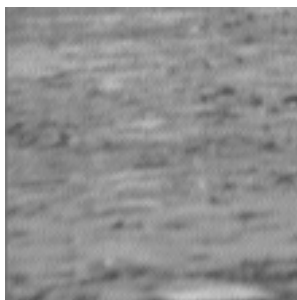


Figure 46: Boat sand part

Table 11: Estimated smoothness of Boat sand part in  $L_2$

smoothness ( $\alpha$ )	-0.3630
norm	0.9595
correlation coefficient	0.9940
error	0.6535

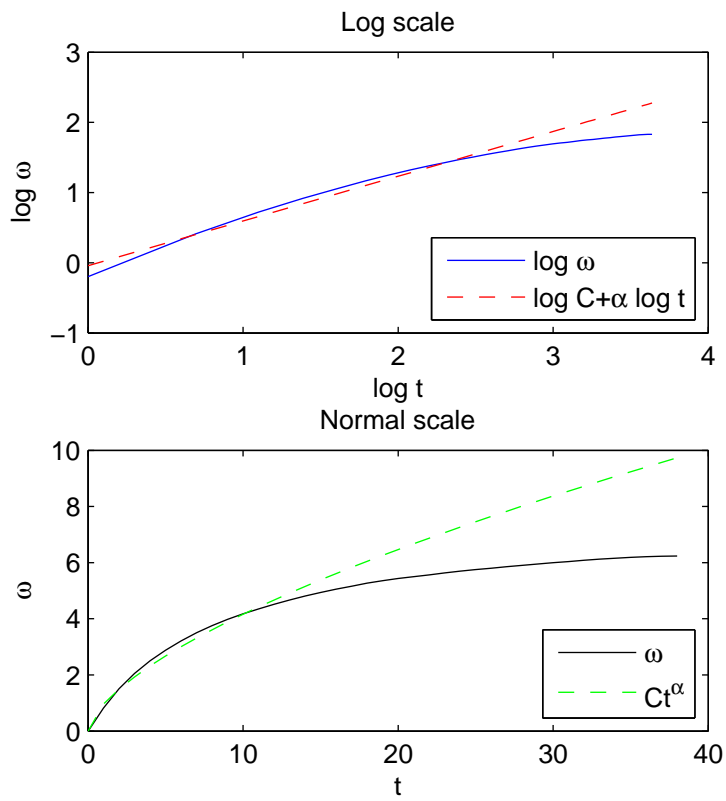


Figure 47: In the first plot, the red dashed line is a least square fit to the log scale of  $\omega$ , the green line, with respect to the small  $t$ . In the second plot one can see the fit of  $\omega$ , black line and  $Ct^\alpha$ , dashed green line, where  $\alpha = -0.3630$  and  $C = 0.9595$  with the  $\mathcal{B}_{\infty,2}^{-0.3630}$ .



Figure 48: Boat geometric

Table 12: Estimated smoothness of Boat geometric part in  $L_2$

smoothness ( $\alpha$ )	0.1586
norm	7.2615
correlation coefficient	0.9978
error	3.2004

---

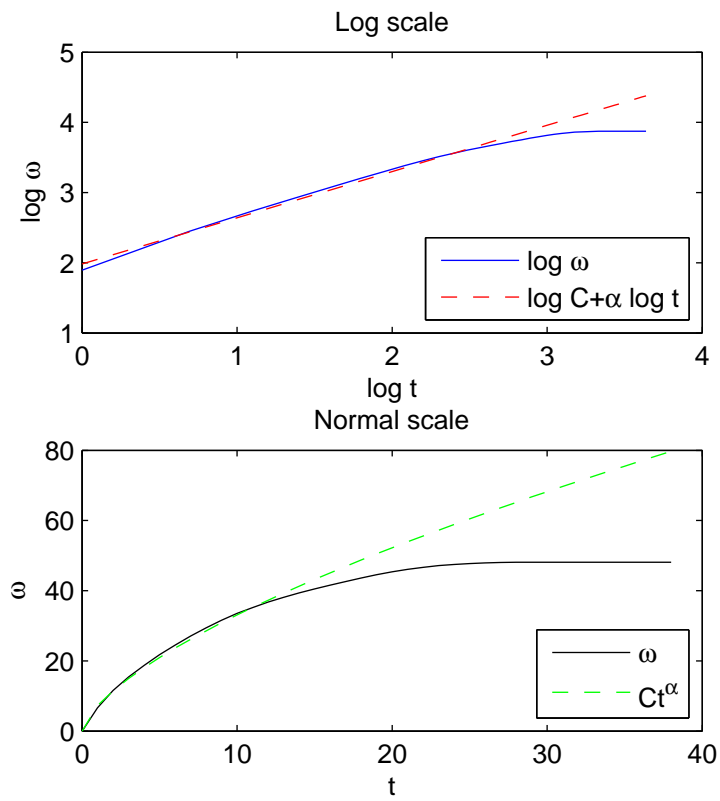


Figure 49: In the first plot, the red dashed line is a least square fit to the log scale of  $\omega$ , the green line, with respect to the small  $t$ . In the second plot one can see the fit of  $\omega$ , black line and  $Ct^\alpha$ , dashed green line, where  $\alpha = 0.1586$  and  $C = 7.2615$  with the  $\mathcal{B}_{\infty,2}^{0.1586}$

## 6 Conclusion and Further study

### 6.1 Conclusion

In chapter 4 of this thesis, the results of the Modulus of continuity method are obtained. One can split the results in two tables, negative (Table 13) and positive (Table 4) smoothness. According to these tables, one can see,

- the geometric part of the images mostly have a positive smoothness,
- the texture part have negative smoothness,
- the smoothness range between  $0.1 < \alpha < 0.3$  and  $-0.4 < \alpha < -0.1$ .

Table 13: Negative smoothness

Part of image	smoothness ( $\alpha$ )
Lenna Hat figure 28	-0.2069
Lenna Hat's Hair figure 32	-0.2765
Mandrill Beard figure 36	-0.3165
Mandrill Hair figure 40	-0.3351
Fruit Skin figure 44	-0.3148
Boat Sand figure 46	-0.3630

Table 14: Positive smoothness

Part of image	smoothness ( $\alpha$ )
Lenna Geometric figure 30	0.2851
Lenna skin figure 34	0.2651
Mandrill nose figure 38	0.220
Fruit Geometric figure 42	0.2052
Boat Geometric figure 48	0.1586

In comparison, Table 15 shows that the author conclude on the same results as Carasso reported in [9]. There is still a small error that can be happend according to the calculaton in MATLAB.

Table 15: Carasso method

		Galaxy M51 Figure20	Mandrill Figure18
Smoothness $\alpha$	Carasso	0.5300	0.3060
	Own approach	0.5227	0.3053

## 6.2 Further study

Finally, from the previous study and this thesis, one can:

1. use the result and model for deblurring, denoising and compression,
2. increase the number of the pixels in the way that the wavelet norm and error have the same result,
3. expand samples and classify different texture spaces.

Unfortunately, there was not more time to go further in this thesis, however it still remains some interesting topics and projects to study for interested researchers and students.

## References

- [1] R. A. DeVore, B. J. Lucier, *Classifying the smoothness of images: theory and application to wavelet image processing* IEEE 0-818606950-0/94.
- [2] R. A. DeVore, B. Jaweth, and B. J. Lucier, *Image Compression Through Wavelet Transform Coding* IEEE, Transaction on Information Theory, VOL.38, NO.2, March 1992.
- [3] A. Chambolle, R. A. DeVore, N. Lee, and B. J. Lucier, *Nonlinear Wavelet Image Processing: Variational Problems, Compression, and Noise Removal Through Wavelet Shrinkage* IEEE Trans. Image Process, 7(1998), pp. 319-335.
- [4] Y. Meyer *Oscillating Patterns in Image Processing and Nonlinear Evolution Equation* Univ. Lecture Ser. 22, AMS, Providence IR, 2001.
- [5] J.-M Morel and Y. Gousseau *Are natural images of bounded variation ?* SIAM J. Math. Anal. ,33 (2001), pp. 634-648.
- [6] J. Bergh, J. Lofsrton *Interpolation Spaces An Introduction* Berlin ; New York : Springer-Vlg, 1976.
- [7] G. W. Recktenwald *Numerical Methods with Matlab: Implementations and Applications* Prentice-Hall, Upper Saddle River, NJ, 2000-2007.
- [8] R. A. Devore, B. Jaweth, and B. J. Lucier, *Data compression using wavelets: error, smoothness and quantization* Extended Abstract.
- [9] A.S.Carasso *Singular integrals, image smoothness, and the recovery of texture in image deblurring* society for industrial and applied mathematics SIAM J. APPL. MATH. Vol.64, No. 5, pp. 1749-1774.
- [10] Y. Meyer, J. B. Granett, T. M. Le, L. A. Vese. *Image decomposition using bounded variation and generalized homogeneous Besov spaces* Elsevier science Inc, doi:10.1016/j.acha.2007.01.005.



# **Linnæus University**

School of Computer Science, Physics and Mathematics

SE-351 95 Växjö / SE-391 82 Kalmar

Tel +46-772-28 80 00

dfm@lnu.se

Lnu.se